Theoretical and Applied Climatology
https://doi.org/10.1007/s00704-019-02830-y

ORIGINAL PAPER

Optimization and evaluation of a monthly air temperature and precipitation gridded dataset with a 0.025° spatial resolution in China during 1951–2011

Hong Zhao[1] · Wei Huang[1] · Tingting Xie[1] · Xian Wu[2] · Yaowei Xie[1] · Song Feng[3] · Fahu Chen[1,4,5]

Received: 11 November 2016 / Accepted: 28 February 2019

Abstract
Gridded climatic datasets with fine spatial resolution can potentially be used to depict the climatic characteristics across the complex topography of China. In this study, we collected records of monthly temperature at 1153 stations and precipitation at 1202 stations in China and neighboring countries to construct a monthly climate dataset in China with a 0.025° resolution (~2.5 km). The dataset, named LZU0025, was designed by Lanzhou University and used a partial thin plate smoothing method embedded in the ANUSPLIN software. The accuracy of LZU0025 was evaluated based on three aspects: (1) Diagnostic statistics from the surface fitting model during 1951–2011. The results indicate a low mean square root of generalized cross validation (RTGCV) for the monthly air temperature surface (1.06 °C) and monthly precipitation surface (1.97 $mm^{1/2}$). The method used variable square root transformation for the spline surface fitting to reduce positive skewness in the measured precipitation values and no variable transformation in air temperature case. This indicates that the surface fitting models are accurate. (2) Error statistics of comparisons between interpolated monthly LZU0025 with the withholding of climatic data from 265 stations during 1951–2011. The results show that the predicted values closely tracked the real true values with values of mean absolute error (MAE) of 0.59 °C and 70.5 mm and standard deviation of the mean error (STD) of 1.27 °C and 122.6 mm. In addition, the monthly STDs exhibited a consistent pattern of variation with RTGCV. (3) Comparison with other datasets. This was done in two ways. The first was via comparison of *standard deviation*, *mean*, and *time trend* derived from all datasets to a reference dataset released by the China Meteorological Administration (CMA), using Taylor diagrams. The second was to compare LZU0025 with the station dataset in the Tibetan Plateau. Taylor diagrams show that the *standard deviation* derived from LZU had a higher correlation with that produced by the CMA (R = 0.76 for air temperature, and R = 0.96 for precipitation) compared to those from other datasets. The standard deviation for the index derived from LZU was more close to that induced from CMA, and the centered normalized root-mean-square difference for this index derived from LZU and CMA was lower. A similar superior performance of LZU was found in the comparison of *mean* and *time trend* derived from LZU and those from other datasets. LZU0025 had high correlation with the Coordinated Energy and Water Cycle Observation Project (CEOP)—Asian Monsoon Project (CAMP) Tibet surface meteorology station dataset for air temperature, despite a non-significant correlation for precipitation at a few stations. Based on this comprehensive analysis, we conclude that LZU0025 is a reliable dataset. LZU0025, which has a fine resolution, can be used to identify a greater number of climate types, such as tundra and subpolar continental, along the Himalayan Mountain. We anticipate that LZU0025 can be used for the monitoring of regional climate change and precision agriculture modulation under global climate change.

✉ Wei Huang
whuang@lzu.edu.cn

[1] Key Laboratory of Western China's Environmental Systems (Ministry of Education), College of Earth and Environmental Sciences, Lanzhou University, Lanzhou 730000, China

[2] Sanming Meteorologic Bureau, Sanming, China

[3] Department of Geosciences, University of Arkansas, Fayetteville, AR 72701, USA

[4] Key Laboratory of Alpine Ecology and Biodiversity (LAEB), Institute of Tibetan Plateau Research, Chinese Academy of Science, Beijing 100101, China

[5] CAS Center for Excellence in Tibetan Plateau Earth Sciences, Beijing 100101, China

Published online: 26 March 2019

1 Introduction

Regional climatic conditions are a primary determinant of agricultural productivity. Changes in temperature and precipitation will result in changes in land and water regimes that may subsequently affect agricultural productivity (Anwar et al. 2013). Over the past century, China has experienced substantial climate change: during the past 100 years, the annual average temperature has increased by 0.5–0.8 °C (Ding et al. 2007) and the distribution of precipitation has become more uneven (Piao et al. 2010; Liu et al. 2018). Agriculture in China is as a major industry, supporting over 20% of the world's population with only 8% of global cultivated area, and it is also a major importer of feed grains in the world market (Chen et al. 2016). Therefore, it is important to understand the impacts of climate change on agriculture in China, both in terms of the welfare of the Chinese population and the influence China has on world food markets. To address this issue, agronomists usually use climatic observation data from weather stations; however, the use of this type of data may lead to site-dependent results and tends to ignore the heterogeneity in a specific geographical unit.

Climatic-gridded datasets, generated from the interpolation of observations, express the distribution of climate over space, and they are widely used in global and regional climate change research. Air temperature and precipitation are the most important basic elements in climatic research. Commonly used global monthly climatic datasets, such as those with 0.5° resolution produced by the Climatic Research Unit (CRU) of the University of East Anglia in the UK (Harris et al. 2014), and by the Climate Prediction Centre (CPC) released by the National Oceanic and Atmospheric Administration (NOAA) (Fan and Van den Dool 2008), have been used to analyze the modern spatial climatic characteristics of China (Wen et al. 2006; Zhou et al. 2010; Huang et al. 2015). However, in the case of these global datasets, climatic observations in only ~200 sites were used for interpolation across the complex terrain of China, and therefore significant biases occur over much of the country (Zhang et al. 2009).

Monthly gridded air temperature and precipitation datasets with 0.5° resolution for mainland China have been developed and released by the China Meteorological Administration (CMA) (http://cdc.nmic.cn/datasets.do?dsid=SURF_CLI_CHN_MUL_MON). These datasets have been used to analyze the response of vegetation phenology to temperature and precipitation (Shen et al. 2015; Xiao et al. 2016) and to assess the variability of climatic conditions for different types of crop and crop yields (Zhao et al. 2014; Li et al. 2015; Song et al. 2015; Liu et al. 2016; Zhang et al. 2016). Agroclimatic research has also used this dataset to investigate the effects of climate change on the cultivated area (Liu et al. 2015). However, the coarse spatial resolution of the CMA dataset makes it difficult to determine the relationship between climate change and agriculture on a regional scale, and in addition, climate regimes in mountainous areas are not captured with sufficient precision. These problems may have significant impact on local agricultural strategies and national decision-making in terms of adapting to climate change. In addition, the CMA only used observations in China, and the quality of the datasets may be reduced for areas close to the national border. Therefore, a set of climatic datasets with high spatial and temporal resolution are needed for applications in regional agroclimatic research, especially the climate impacts on agriculture in mountainous areas. Monthly air temperature and precipitation datasets with 0.025° resolution have been constructed and improved for mainland China with the production of our preliminary dataset (Wu et al. 2014); however, the interpolated data are confined to China. Consequently, the objectives of the present research are (1) optimization of LZU0025 by extending the station data to neighboring countries and (2) assessment of the accuracy of LZU0025 using three approaches: analysis of surface diagnostic statistics to assess the spline interpolation model, analysis of errors by comparing interpolated values to withheld station data, and comparison of LZU0025 with existing datasets.

2 Data and methods

2.1 Data

We used the monthly air temperature and precipitation dataset from the "China ground monthly climate dataset", based on 753 national meteorological stations (Fig. 1). Its quality and uniformity are evaluated by the National Meteorological Information Center (Feng et al. 2004; Li et al. 2004). Besides the observations in China, the monthly air temperature data on 405 stations and monthly precipitation data on 449 stations from the neighboring countries (such as India, Mongolia, etc.), obtained from the Global Historical Climate Network (GHCN-Monthly Version 3), were also used in this study (Fig. 1). The quality of the extended station data, such as the presence of duplicate or overflow data (where the value exceeds the mean plus 5 standard deviations) in consecutive months, was checked automatically and inhomogeneous data were removed by using the Pairwise Homogeneity Algorithm (PHA) software (Menne and Williams 2009). The internal consistency such as air temperature in the cooler periods is lower than that in warm periods was also checked (Feng et al. 2004). However, the elevation data at some sites were missing. As the elevation is of great importance for the accuracy of data interpolation, the missing elevation data for some GHCN stations were derived from the global 90 m digital elevation data. In addition, digital elevation data covering China and its neighboring areas was required. Owing to the spatial coverage and temporal continuity of Chinese meteorological station

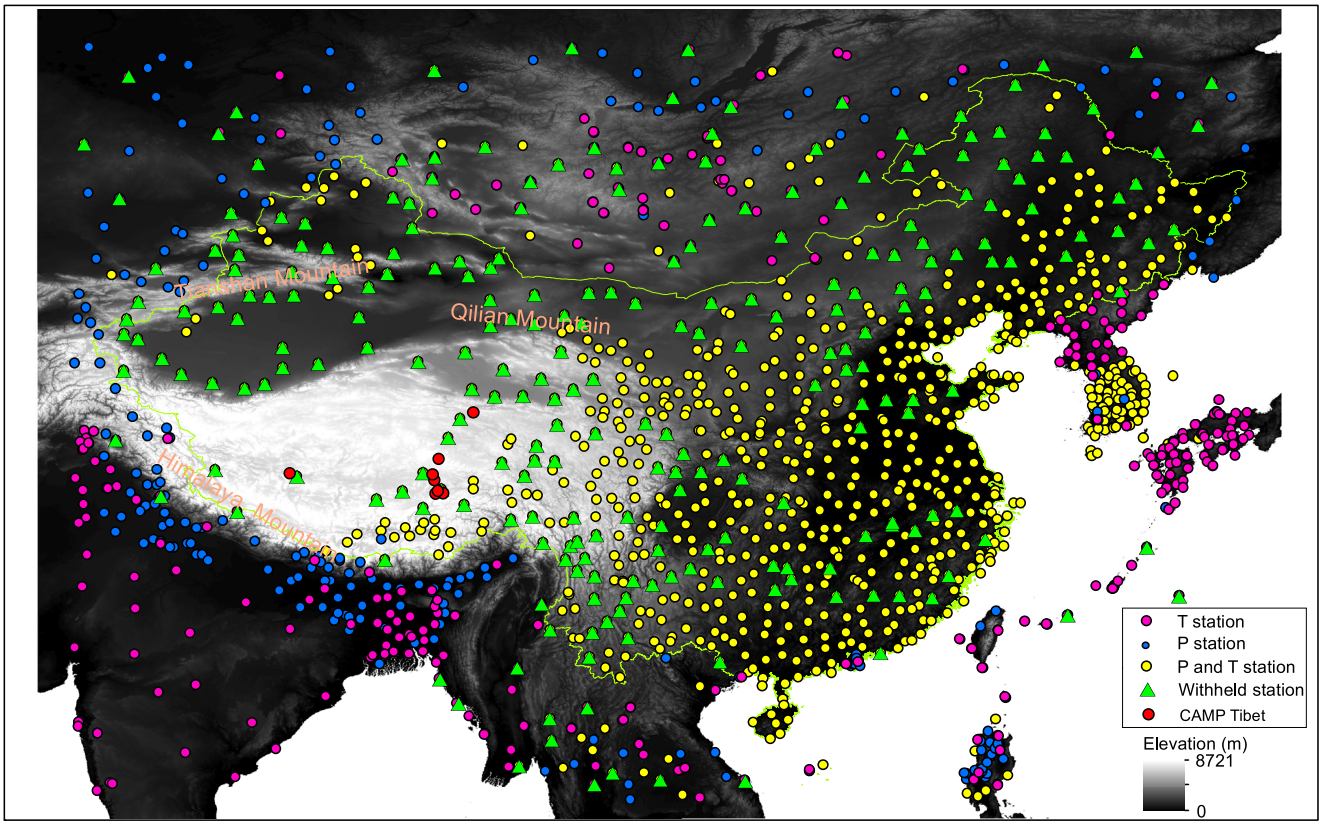

Fig. 1 Distribution of air temperature and precipitation stations. The blue circle dots represent for precipitation stations, red dots for the air temperature stations, and yellow dots for the stations where both precipitation and air temperature were measured. The green triangles represent the withheld stations and the red dot refers to the Coordinated Energy and Water Cycle Observation Project (CEOP)-Asian Monsoon Project, CAMP Tibet surface meteorology stations. The background is the digital elevation map describing the elevation in this area

data and the recent updated GHCN-Monthly datasets occurring in 2011 (https://www.ncdc.noaa.gov/ghcnm/v3.php), we focused on dataset optimization from Jan 1951 to Dec 2011.

To assess the accuracy of the new updated LZU0025, several published and widely used monthly air temperature and precipitation products were used for comparisons (Table 1). Station-based interpolation products involved CPC, CRU, CMA, and the University of Delaware Air Temperature and Precipitation product (hereafter UD). These datasets contain both air temperature and precipitation elements. Since atmospheric reanalysis data are commonly used in studies of climate change, energy balance, and the hydrological cycle, surface monthly air temperature product from the National Centers for Environmental Prediction (hereafter NCEP) and the ERA-Interim 2-m temperature product from the European Centre for Medium-Range Weather Forecasts (hereafter ECMWF) were also collected. For precipitation element, Global Precipitation Climatology Centre (GPCC) monthly product and Asian Precipitation-Highly-Resolved Observational Data Integration Towards Evaluation monthly dataset (APHRO) derived from the APHRO_MAV1101R2 daily dataset were used. In addition, CMA was taken as a benchmark for comparisons since its interpolation is based on 2472 ground meteorological stations, including unpublished local stations in China (SURF_CLI_CHN_TEM_MON_GRID_0.5). Besides, the fine scale, the goal of the Coordinated Energy and Water Cycle Observation Project (CEOP)-Asian Monsoon Project, CAMP Tibet surface meteorology station dataset (hereafter CAMP Tibet, in Fig. 1) (Ishikawa 2011) in available period of 2003–2004 (https://data.eol.ucar.edu/dataset/list/) was also used.

2.2 Method

Thin plate spline interpolation is well-suited for the interpolation of monthly air temperature and precipitation datasets (Hutchinson et al. 2009). This method provides accurate estimates of climate by allowing for the spatially varying dependence on topography, and it is able to provide a direct estimation of interpolation error, as well as efficient diagnosis of data errors (Hutchinson and Gessler 1994). The underlying statistical model is as follows (Wahba and Wendelberger 1980; Wahba 1983; Wahba 1986; Wahba 1990; Hutchinson 1993; Hutchinson and Xu 2004; Hutchinson and Xu 2013)

$$z_i = f(\boldsymbol{x}_i) + \boldsymbol{b}^T \boldsymbol{y}_i + e_i (i = 1, \ldots, N) \quad (1)$$

Table 1 Summary of air temperature and precipitation datasets

Dataset	Sources	Variable	Spatial resolution	Time span	Reference
CPC	The Climate Prediction Center, National Centers for Environmental Prediction	T/P	0.5*0.5°	1948–2015	Fan and Van den Dool (2008)
UD	Center for Climatic Research Department of Geography, University of Delaware Newark, USA	T/P	0.5*0.5°	1901–2008	Matsuura and Willmott (2009)
CRU	University of East Anglia Climatic Research Unit, UK	T/P	0.5*0.5°	1901–2009	Harris et al. (2014)
LZU	University of Lanzhou, China	T/P	0.5*0.5°	1961–2011	
CMA	China Meteorological Administration, China	T/P	0.5*0.5°	1961–2015	Xu et al. (2009)
NCEP	NOAA National Center for Environmental Prediction	T	2.5*2.5°	1948–2015	Kalnay et al. (1996)
ECMWF	The European Centre for Medium-Range Weather Forecasts, Europe	T	0.5*0.5°	1979–2015	Dee et al. (2011)
APHRO	APHRODITE's Water Resources, Japan	P	0.5*0.5°	1951–2007	Yatagai et al. (2012)
GPCC	Deutscher Wetterdienst, Germany	P	0.5*0.5°	1901–2010	Schneider et al. (2011)

T is the abbreviation of air temperature and *P* is that of precipitation

where z_i is the dependent variable (i.e., air temperature and precipitation) at location i. $\boldsymbol{x}_i$ is a d-dimensional vector of spline independent variables, where d is the number of spline variables. $f(\boldsymbol{x}_i)$ is an unknown smooth function of $\boldsymbol{x}_i$. The method of only using smooth function to do the interpolation is called the thin spline smoothing splines (Wahba and Wendelberger 1980). In the precipitation interpolation case, besides taking latitude and longitude as $\boldsymbol{x}_i$, the elevation was recommended being incorporated as the third independent variable to consider orographic effect on precipitation distribution, and this would make a big contribution to surface interpolation accuracy (Hutchinson 1995). To allow for additional dependencies that have physical influences on climate variable, a linear parametric sub-model of $\boldsymbol{b}^T\boldsymbol{y}_i$ is added to smooth function, and this semi-parametric model is called as partial thin plate splines (Wahba 1990). In which $\boldsymbol{y}_i$ is a p-dimensional vector of independent linear covariate (i.e., dependency), where p is the number of covariates, and $\boldsymbol{b}^T$ is an unknown p-dimensional vector of coefficients of $\boldsymbol{y}_i$. Since temperature decline approximately linearly with elevation (Houghton 2002), in the temperature interpolation case, elevation above the sea-level was used in the interpolation as an independent covariate $\boldsymbol{y}_i$ and $\boldsymbol{y}_i$ became one-dimension. The coefficient of an elevation covariate could be assumed as an empirically determined temperature lapse rate (Hutchinson 1991). The interpolated surface would reflect the temperature variation in vertical visually high mountainous region, with the obvious elevation changing character (Zhang et al. 2011). Each e_i is an independent and zero mean error term with the variance $w_i\sigma^2$, where w_i is termed of the relative error variance and was set uniformly weighted for each surface and σ^2 is the error variance (unknown) that is constant across all data points (Hutchinson 1991). N is the number of data point, with $N = 1158$ in temperature case and $N = 1202$ in precipitation case. The function f and coefficient vector $\boldsymbol{b}$ are determined by minimizing

$$\sum_{i=1}^{N}\left[\frac{Z_i - f(\boldsymbol{x}_i) - \boldsymbol{b}^T\boldsymbol{y}_i}{w_i}\right]^2 + \rho J_m(f) \tag{2}$$

where $J_m(f)$ is a measure of the complexity of f, the "roughness penalty" defined in terms of an integral of mth order partial derivatives of f. The estimate of f having an expansion in terms of scalar function of distance from each data position and the form of the scalar function depend on the dimension of the $\boldsymbol{x}_i$ and the m (Wahba 1990). w_i is the relative variance and was set as the uniform for each surface. ρ is a positive number called the smoothing parameter, determining a trade-off between data infidelity and surface roughness (Hutchinson 1991; Hutchinson 1993). As ρ approaches zero, the fitted function approaches an exact interpolant. As ρ approaches infinity, the function f approaches a least squares polynomial, with order depending on the order m of the roughness penalty. The value of the smoothing parameter ρ is normally determined by minimizing a measure of predictive error of the fitted surface given by the generalized cross validation (GCV) (Hutchinson and Gessler 1994). When more stations are distributed evenly used in Eqs. (1) and (2), more detailed surface fitting could be obtained in terms of GCV criteria. Figure 1 shows that 1158 air temperature stations and 1202 precipitation stations covering the area of China and its neighboring countries were used to fit the climatic surface. The knots chosen from the data points with number of 1/4 to 1/3 of the size of the dataset were chosen to be used to limit the complexity $J_m(f)$ of the fitted surface. With more stations data used for surface fitting, more knots were selected and the fitted surface could be more close to real complex terrain in China. In this paper, due to meteorological data privacy

policy, only above limited numbers of available stations data were used for interpolation for such a large area.

The vector $\hat{z}$ of fitted function values can be written as (Hutchinson and Xu 2004)

$$\hat{\boldsymbol{z}} = \boldsymbol{A}\boldsymbol{z} \tag{3}$$

where $\hat{\boldsymbol{z}}$ is a vector of all grid points (N) values of air temperature or precipitation, and $\boldsymbol{z}$ is corresponding observed value. $\hat{\boldsymbol{z}}$ and $\boldsymbol{z}$ is connected through $\boldsymbol{A}$, an $N \times N$ matrix called the *influence matrix* (Hutchinson and Xu 2004). The number of degrees of freedom of the fitted spline is defined as SIGNAL (= trace ($\boldsymbol{A}$), unit: dimensionless), and the number of degrees of freedom of the weighted residual sum of squares is given as ERROR (= N–trace ($\boldsymbol{A}$)).

The weighted mean residual sum of squares (MSRs) is given by (Hutchinson and Xu 2004)

$$\mathrm{MSR} = \left\| \boldsymbol{W}^{-1}(\boldsymbol{I}-\boldsymbol{A})\boldsymbol{z} \right\|^2 / N \tag{4}$$

where $\| \|^2$ means to square the norm of residuals, and $\boldsymbol{I}$ is the identity matrix. $\boldsymbol{A}$, $\boldsymbol{z}$ and N share the same meanings with Eq. 3. $\boldsymbol{W}$ is the diagonal matrix given by

$$\boldsymbol{W} = \mathrm{diag}(w_1, \ldots . w_n) \tag{5}$$

The GCV is calculated for each value of the smoothing parameter ρ by implicitly removing each data point and calculating the residual from the omitted data point of a surface fitted to all other data points using the same value of ρ. The GCV is then a suitably weighted sum of the squares of these residuals (Craven and Wahba 1978; Wahba 1990). The GCV is calculated by the formula (Hutchinson and Xu 2004)

$$\mathrm{GCV} = \frac{\left\| \boldsymbol{W}^{-1}(\boldsymbol{I}-\boldsymbol{A})\boldsymbol{z} \right\|^2 \Big/ N}{\left[trace(\boldsymbol{I}-\boldsymbol{A}) \Big/ N \right]^2} \tag{6}$$

When the surface fitting procedure fails to obtain the smoothing parameter, an asterisk in the output log file flags the SIGNAL (Hutchinson and Xu 2004). Hutchinson (1993) and Hutchinson and Gessler (1994) recommend that the SIGNAL should not exceed about half the number of data points. SIGNAL larger than this can indicate insufficient data or positive correlation in data errors. The GCV and MSR are read from the output log file together with their square roots RTGCV and RTMSR. A reliable model is suggested by having SIGNAL not exceeding half the number of data points and having low RTGCV and RTMSR.

The value $\hat{z}_i$ of a spline surface at an arbitrary position i can be written as (Hutchinson and Xu 2004)

$$\hat{z}_i = \boldsymbol{a}_i^T \boldsymbol{c} \tag{7}$$

where $\boldsymbol{a}_i$ is a vector depending on i. $\boldsymbol{c}$ is the vector of surface coefficient. The standard error estimate of the surface value $\hat{z}_i$ (also called the model standard error) is calculated using the formula

$$\left(\boldsymbol{a}_i^T v \boldsymbol{a}_i \right)^{1/2} \tag{8}$$

where v is the error covariance of surface coefficient $\boldsymbol{c}$. With considering the error in estimating the model given by Eq. (1), the predicted standard error (SE) is calculated using the formula

$$\mathrm{SE} = \left(\boldsymbol{a}_i^T v \boldsymbol{a}_i + \sigma^2 \right)^{1/2} \tag{9}$$

where σ^2 is the variance of the data error e_i in Eq. (1) and the data error variance (VAR) can be estimated by

$$\mathrm{VAR} = \frac{\left\| \boldsymbol{W}^{-1}(\boldsymbol{I}-\boldsymbol{A})\boldsymbol{z} \right\|^2}{trace(\boldsymbol{I}-\boldsymbol{A})} \tag{10}$$

The flow chart for generating a climatic dataset is illustrated in Fig. 2. Taking preprocessed station dataset and DEM data as the input, considering the amount of dataset < 2000 (Hutchinson and Xu 2004), the SPLNEA was employed to calculate the surface coefficient and its error covariance. The surface diagnostic files for the GCV calculation and large residual file for data error check were also output as with the log file recording a set of indices on evaluating whether perfect surface fitting was reached. It is noted that in precipitation case, to reduce the skew in the raw data, the square roots of the monthly rainfalls was interpolated and then the interpolated values were squared. The units of corresponding surface statistic diagnostic such as the square roots—RTGCV, RTMSR, and RTVAR—for precipitation interpolation should the square root mm ($\mathrm{mm}^{1/2}$) (Hutchinson 1998a).

When surface fitting parameters in Eqs. (1) and (2) were estimated by using the SPLNEA module, with the implementation of digital elevation model (DEM) providing latitude, longitude, and elevation information in a grid cell, the fitted climatic values and corresponding predicted standard error (see Eq. (9)) in the grid were calculated by using the LAPGRD module. Therein, the back-transformation of precipitation fitted surfaces was implemented. As the surface complexity f was estimated relating to distance from each data position (see Eq. (2)), the closest interpolated stations had the distance of approximately 6 km and this value could be taken as the minimum spatial resolution in theory (Hutchinson 1998b). While NASA's Jet Propulsion Laboratory (JPL) provides global DEM with approximate 90 m resolution (https://cgiarcsi.community/data/srtm-90m-digital-elevation-database-v4-1/). This explicit geographic information might be used for getting the fitted surface in the sub-grid that could match the spatial resolution of commonly used land state datasets such as the Moderate Resolution

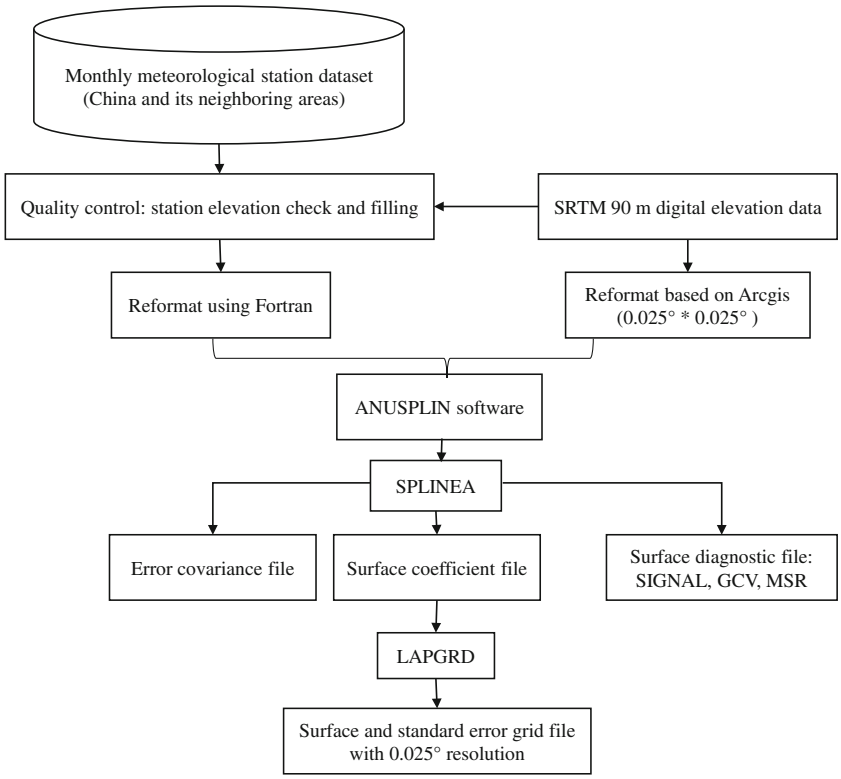

Fig. 2 Flow chart for constructing the LZU0025 gridded monthly air temperature and precipitation datasets

Imaging Spectroradiometer (MODIS) Leaf Area Index 1 km dataset (https://ladsweb.modaps.eosdis.nasa.gov/missions-and-measurements/products/lai-and-fpar/MYD15A2/) and satellite soil moisture 3 km dataset (https://nsidc.org/data/smap/smap-data.html). Considering computational efficiency, as a tradeoff, monthly air temperature and precipitation dataset and their corresponding error dataset with a 0.025° resolution (~2.5 km) were generated.

Besides using surface diagnostic (e.g., RTGCV) to assess the accuracy of interpolation model, residuals from stations withheld from the interpolation were examined. Considering approximate 1/3 of the size of dataset as withheld data, 700 air temperature and precipitation stations were selected by using SELNOT program in the ANUSPLIN package. This program removed points from the closest pairs in the dataset and led to three-dimensional space scaled to have unit variance. Given the site maintenance in the entire time period, 435 air temperature stations and 373 precipitation stations were kept and with 265 stations (shown in Fig. 1) sharing. These 265 stations were used as the withheld to assess the accuracy of interpolation. The mean error (ME), mean absolute error (MAE), and standard deviation of mean error (STD) were calculated by using the ANUSPLIN-interpolated values against the withheld station data.

To further evaluate the accuracy of the climatic datasets, comparisons were made with global climatic datasets (Yatagai et al. 2012; Pai et al. 2014; Schneider et al. 2014; Yu et al. 2015). Statistical indicators of correlation and bias and the spatial distribution of climatic parameters are usually calculated and compared to assess the datasets (Conti et al. 2014; Wu et al. 2014; Ciabatta et al. 2015; Hessels 2015; Yu et al. 2015). It should be noted that comparisons are mainly based on mean states, while comparatively few are based on deviations from the average. In order to thoroughly evaluate the new LZU0025 datasets, we used statistical indices—the *mean* reflecting average climate status, the *standard deviation* from the mean that can depict anomaly, and the *time trend* describing changes of precipitation and air temperature with time (Eq. (11))—as the bases for comparison.

$$\begin{aligned} mean_{\mathrm{i}} &= \frac{1}{\mathrm{T}}\sum_{\mathrm{t}}^{\mathrm{T}} \mathrm{r}_{\mathrm{i}}^{\mathrm{t}} \\ standard\ deviation_{\mathrm{i}} &= \sqrt{\frac{1}{\mathrm{T}}\sum_{\mathrm{t}}^{\mathrm{T}}\left(\mathrm{r}_{\mathrm{i}}^{\mathrm{t}}-\overline{\mathrm{r}}_{\mathrm{i}}\right)^{2}} \\ \text{time trend}_{\mathrm{i}} &= (\text{regression coefficient})_{\mathrm{i}} \end{aligned} \tag{11}$$

where r_i^t is the value of climatic element at a grid i with monthly time index t (1,2,3,….,T), and T is the total amount of months in the whole time period. $\bar{r}_i$ is the mean value during the whole time period at the grid i. The *time trend*$_i$ equals to the linear regression coefficient derived from regressing all values in time series at the grid i. The RegCoef command in NCAR Common Language was used to calculate linear regression coefficient, and 95% confidence limits were constructed for the regression coefficient (https://www.ncl.ucar.edu/Document/Functions/Built-in/regCoef-1.shtml).

The Taylor diagram (Taylor 2001; Taylor 2005) is an effective way of graphically illustrating how closely a set of patterns match observation in a single graph and has been used to assess the performance of atmospheric model simulations (Brown et al. 2011; IPCC 2013; Kim et al. 2013; Ma et al. 2014). However, Taylor diagrams have not been used to evaluate the accuracy of gridded datasets. In this paper, we constructed Taylor diagrams for the *mean*, the *standard deviation* from mean, and the *time trend* derived from all datasets to evaluate the accuracy of the new LZU0025 dataset.

In the Taylor diagram, the difference between targeted dataset and the reference is characterized in terms of their Pearson correlation (R), their centered normalized root-mean-square difference (RMSE), and the ratio of their standard deviations STD_{ratio} ((Eq. (12), below). STD is taken as the radius in the graph. R is represented by cosine of the angle of a polar plot, and the distance to the reference point is the RMSE. With being close to the reference point in Taylor diagram, targeted dataset is demonstrated becoming similar to the reference from the perspective of used index (e.g., *mean*). The targeted dataset located at the x-axis with R = 1 and STD_{ratio} = 1 has a perfect similarity with the reference. When targeted dataset is positioned close to the reference in all Taylor diagrams constructed from *mean*, *standard deviation*, and *time trend*, this dataset is concluded reliable. The formulas used for figuring Taylor diagram are as follows:

$$R = \frac{\frac{1}{s}\sum_{i=1}^{s}\left(n_i-\overline{n}\right)\left(m_i-\overline{m}\right)}{STD_n * STD_m}$$

$$\mathrm{RMSE} = \frac{\sqrt{\frac{1}{s}\sum_{i=1}^{s}\left[\left(n_i-\overline{n}\right)-\left(m_i-\overline{m}\right)\right]^2}}{STD_m}$$

$$STD_n = \sqrt{\frac{1}{s}\sum_{i=1}^{s}\left(n_i-\overline{n}\right)^2} \quad STD_m = \sqrt{\frac{1}{s}\sum_{i=1}^{s}\left(m_i-\overline{m}\right)^2}$$

$$STD_{ratio} = \frac{STD_n}{STD_m} \tag{12}$$

where m_i refers to the index (i.e., *standard deviation*, *mean*, and *time trend*, see Eq. (11)) at grid of *i* derived from the reference CMA, and n_i represents the index at grid of *i* derived from other datasets. $\overline{n}$ and $\overline{m}$ are the mean values in space, and *s* is the total number of grids in the whole China area. Here, the normalized Taylor diagrams were used with the reference (abbreviated as REF in the figure) plotted on the x-axis at unit distance from the origin. The normalized REF has $R = 1$, $STD_{ratio} = 1$ and RMSE = 0.

To make comparisons at the same spatial scale, the resolution of LZU0025 was up-scaled to 0.5° using the nearest neighbor method. The value of a grid from LZU0025 that was closest to the grid from CAM with the resolution of 0.5° was used to assign a value to this grid. The resampled dataset was named LZU. Other products were resampled using bilinear interpolation to enable comparison with CMA. Besides, mean climate values in time series derived from all dataset were figured for comparisons, and the spatial distributions of climatological annual mean air temperature and precipitation derived from datasets were also illustrated for assessing the accuracy of LZU0025. Last but not the least, the CAMP Tibet meteorology station dataset was used to evaluate the accuracy of LZU0025 on mountainous remote area. The Pearson correlation was calculated to measure how highly correlated are LZU0025 and CAMP Tibet after going through significant test. Higher correlation greater than 0.7 (considered as strong correlation in statistics) indicates that the interpolated LZU0025 could provide climatic values close to measured values. The mean bias was also calculated for comparisons.

3 Results and discussion

3.1 Model performance in ANUSPLIN

Diagnostic statistics for air temperature and precipitation surface fitting during 1951–2011 period were extracted from log files after running SPLINEA module (see Fig. 2). Table 2 shows that the mean smoothing parameter ρ almost reached zero, indicating an exact interpolant occurring. The mean values for SIGNAL do not exceed half the number of data points, demonstrating a successful surface model constructed. The mean SIGNAL values also exhibit a smooth transition from 1 month to another, with the highest value in winter and the smallest in summer. The interpolation error RTGCV for the monthly air temperature surface averaged of 1.06 °C, and it also exhibited monthly change with smallest error predominantly occurring in summer and the greatest in winter. The RTGCV for the monthly precipitation surface averaged of 1.97 $mm^{1/2}$ but was with the greatest error occurring in summer and the smallest in winter. Additionally, the square roots of the weighted mean residual sum of squares (RTMSR) and the data error variance (RTVAR) (see Eqs. (4) and (10) in Sect. 2.2) are low in both cases, indicating the accurate interpolation model and low estimated data error (RTVAR $\leq$ 2.62 $mm^{1/2}$). The spatial pattern of the mean predicted standard error (SE, see Eq. (9)) of monthly air temperature from 1951 to 2011 in Fig. 3a shows low errors ranging of 0.7–1.1 °C from thin plate spline interpolation. The data error of monthly temperature from meteorological stations had a small magnitude of variation (see RTVAR in Table 2). The model error was dominated (see RTGCV in Table 2), and the GCV calculation (see Sect. 2.2) would make GCV higher at station than in surroundings. Therefore, a local error pattern that the interpolated station had a higher SE than surroundings existed in temperature interpolation case (Fig. 3a).

Table 2 Summary statistics for monthly air temperature and precipitation spline surface fitting by means of the method of thin plate spline interpolation during 1951–2011 period

Month	Temperature case					Precipitation case				
	ρ	SIGNAL	RTGCV(°C)	RTMSR(°C)	RTVAR(°C)	ρ	SIGNAL	RTGCV($mm^{1/2}$)	RTMSR($mm^{1/2}$)	RTVAR($mm^{1/2}$)
Jan	0.01	686	1.43	0.37	0.66	0.03	388	1.25	0.82	0.99
Feb	0.01	669	1.28	0.35	0.62	0.03	374	1.27	0.83	1.01
Mar	0.02	588	1.08	0.36	0.61	0.03	387	1.48	0.95	1.16
Apr	0.05	493	0.99	0.43	0.65	0.03	339	1.78	1.21	1.46
May	0.05	502	0.95	0.40	0.62	0.04	318	2.13	1.48	1.77
Jun	0.04	526	0.95	0.39	0.60	0.04	304	2.68	1.90	2.26
Jul	0.04	514	0.91	0.38	0.58	0.04	297	3.10	2.22	2.62
Aug	0.06	481	0.88	0.40	0.59	0.05	268	3.01	2.24	2.60
Sep	0.12	392	0.89	0.49	0.65	0.06	274	2.50	1.85	2.14
Oct	0.11	415	0.93	0.52	0.67	0.04	329	1.95	1.34	1.60
Nov	0.05	516	1.10	0.47	0.69	0.02	433	1.37	0.81	1.04
Dec	0.02	639	1.33	0.39	0.69	0.02	436	1.17	0.71	0.89
Average	0.05	535	1.06	0.41	0.64	0.04	346	1.97	1.36	1.63

The mean error (ME), mean absolute error (MAE), and standard deviation of mean error (STD) based on comparisons between LZU0025 and withheld data during 1951–2011 period were summarized by monthly scale in Table 3. The values were consistent with surface diagnostics in Table 2. Predicted values of monthly air temperature closely tracked the real true values. Mean absolute errors (MAEs) varied in the range of 0.48–0.65 °C, with an overall average of 0.59 °C. This indicated that LZU0025 provided higher monthly air temperature compared to measurements. Standard deviation of errors (STDs) were 1.27 °C in average, in close agreement with mean value of RTGCV values (1.06 °C in Table 2). MAE and STD had a slight monthly variation with errors smaller in winter and greater in summer, which were opposite with RTGCV monthly changing, while they were confined to 1.40 °C.

ME for monthly precipitation errors in Table 3 averaged around 19.1 mm, MAE averaged around 70.5 mm, and STD of 122.6 mm. The root square of average STD was significantly larger than the RTGCV of 1.97 $mm^{1/2}$ in Table 2. The high spatial complexity of daily precipitation might lead to errors in the monthly precipitation surfaces, although these are somewhat ameliorated when they are summed to monthly totals. On the other hand, RTGCV was derived based on the main data network that was dominated by low-elevation stations, while STD was calculated using the withheld data that were sampled with higher elevation gradient. Comparing with temperature, the monthly precipitation withheld errors showed the same seasonal variation exhibited by the RTGCV values (Table 2), with errors greatest in summer and autumn and smallest in winter. Furthermore, there was a great variation of the data error (see RTVAR in Table 2) as well as of the model error (see RTGCV in Table 2), and these two types of errors varied consistently. This would lead to total error (i.e., SE) superposition, and its variation had a same pattern with data error. The spatial pattern of mean SE of monthly precipitation from 1951 to 2011 is displayed in Fig. 3b, which shows the error corresponded to precipitation itself, with error in the northwest less than in the southeast. Due to data error variance of monthly precipitation could exceed 100 mm over the southeast of China in summer season, the SE in Fig. 3b provided values greater than 100 mm. Moreover, the predicted error of precipitation on the mountainous region (e.g., Tianshan and Qilian) showed similar pattern with elevation changing (see Fig. 1), namely greater values on high-altitude area and low errors on neighboring flat regions. This indicated the usability of LZU0025 monthly precipitation dataset, although the Tibetan Plateau region had higher errors in both interpolation cases due to less available meteorological stations (see Fig. 3). While it is noted that the spatial distribution of SE differed between in air temperature and precipitation interpolations (see Fig. 3), and this phenomenon was firstly reported. In summary, the statistics based on surface fitting modeling and comparisons between interpolated LZU0025 with withheld station data demonstrated the accuracy of LZU0025.

3.2 Comparisons with other datasets

Comparisons of the monthly air temperature datasets were made during 1979–2008 period, since the ECMWF dataset initially updated in 1979 and the UD dataset was updated until 2008. Figure 4 illustrates a Taylor diagram comparing the *mean* state, *standard deviation* from mean state, and *time*

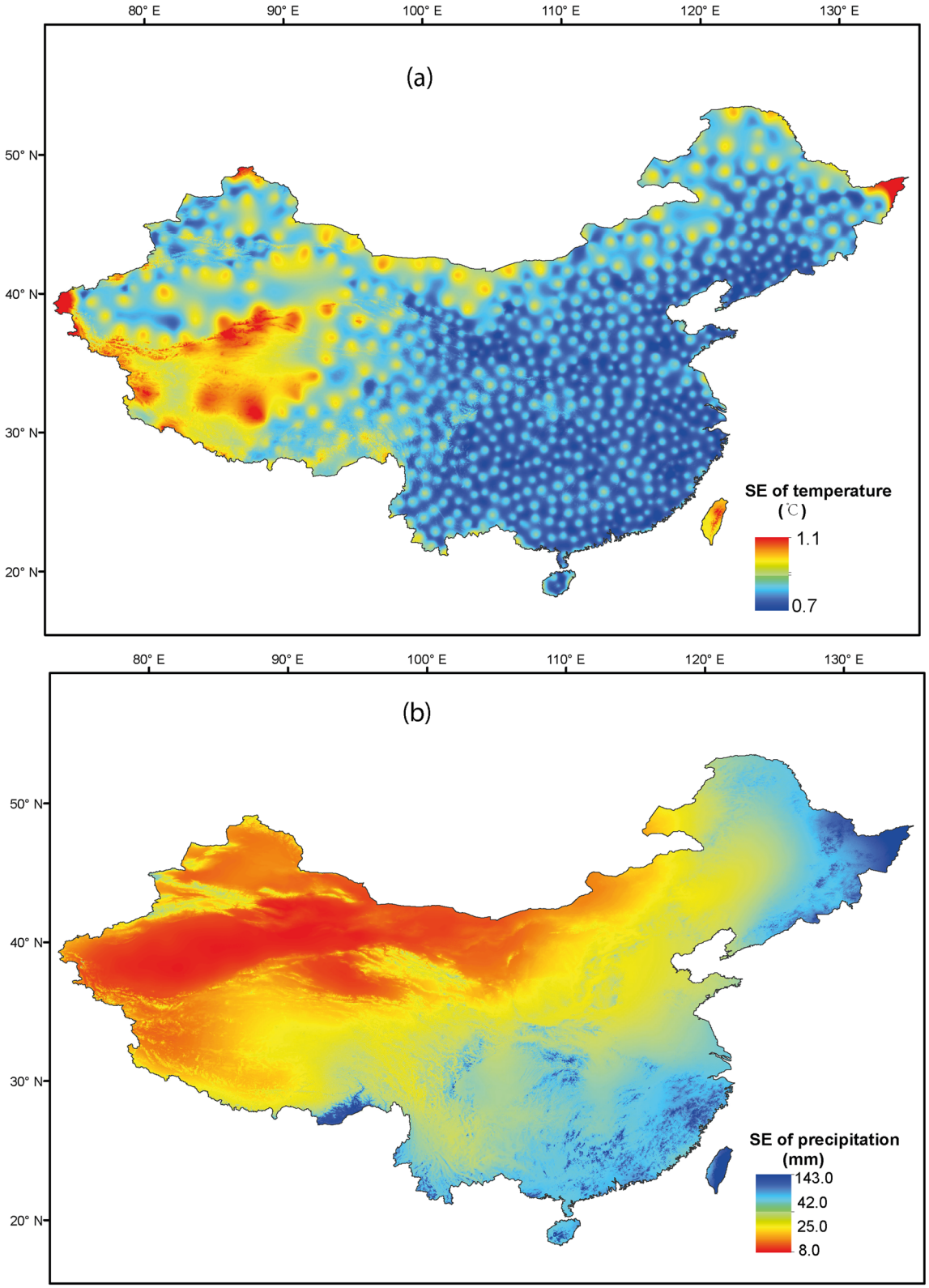

Fig. 3 Spatial distribution of the mean monthly predicted standard error (SE) of climatic elements during 1951–2011 period from the ANUSPLIN. **a** is for air temperature and **b** is for precipitation. The SE contains the model error of spline surface fitting and the estimated data error (see Eq. (9)). Red zones represent a smaller absolute error, while dark blue and cyan areas stand for greater error. The 1:25,000,000 was the digital scale for the map produced by ArcMap software

Table 3 Error statistics of interpolated monthly air temperature and precipitation LZU0025 datasets compared to withheld station data during 1951–2011 period

Month	Temperature (°C)			Precipitation (mm)		
	MAE	ME	STD	MAE	ME	STD
Jan	0.48	0.10	1.04	22.7	7.5	47.9
Feb	0.53	0.11	1.16	27.7	7.1	46.8
Mar	0.59	0.13	1.31	43.5	12.0	73.0
Apr	0.64	0.13	1.35	61.8	25.1	101.0
May	0.62	0.13	1.38	96.3	24.4	151.4
Jun	0.62	0.11	1.40	130.9	33.1	248.3
Jul	0.62	0.10	1.37	131.0	44.7	217.5
Aug	0.63	0.09	1.35	118.7	31.3	191.4
Sep	0.65	0.10	1.32	94.8	23.2	162.5
Oct	0.63	0.11	1.28	63.8	5.9	133.4
Nov	0.57	0.11	1.17	32.5	6.4	58.3
Dec	0.53	0.10	1.07	21.9	8.5	39.4
Average	0.59	0.11	1.27	70.5	19.1	122.6

trend indices (see Eq. (11)) derived from various air temperature datasets. For the *standard deviation* index, Fig. 4a reveals that the correlations of UD and LZU with CMA respectively are the highest (R > 0.75), followed by CRU and ECMWF (R = 0.7–0.75), while for NECP and CPC, it is relatively low (R = 0.6–0.7). The standard deviation (STD) of this index of *standard deviation* indicates that UD is the closest to CMA (STD_{ratio} = 1.1), while CRU, ECMWF, and LZU are closer to CMA (STD_{ratio} = 0.8, 0.9, and 1.25) compared with CPC and NCEP. The RMSE of the *standard deviation* index (dotted semi-circle) shows that the value for UD with CMA is less than 0.75; CRU, ECMWF, and LZU are close to 0.75; and CPC and NCEP are greater than 0.75. The *standard deviation* index indicates that UD is more similar to CMA, followed by LZU, CRU, and ECMWF, and there is a large difference between CMA with CPC and NCEP. For the *mean* index (Fig. 4b), the correlations of LZU and the other datasets with CMA are very high (R = 0.95), and all of the STDs are consistent with that from CMA; however, the RMSEs are less similar but with low values less than 0.5. Thus, from the perspective of the *mean* index, LZU is consistent with other existing datasets. For the *time trend* index (Fig. 4c), the correlations of all of the datasets with CMA are low (R = 0.4–0.7). LZU and UD have the highest correlation coefficient with CMA (R > 0.6), followed by CRU and CPC; and ECMWF and NCEP have the lowest. The STDs of CRU, ECMWF, and NCEP are closer to CMA (STD_{ratio} = 1.25), followed by LZU and UD; CPC exhibits the greatest discrepancy with CMA. The RMSEs of all of the datasets, except for CPC, are close to that of CMA. In terms of the *time trend* index, with the exception of CPC, all of the datasets are similar to CMA. In summary, the CRU, UD, LZU, and ECMWF datasets are more similar to CMA, and CPC and NCEP exhibit the greatest differences to CMA.

Next, we evaluate spatial distributions of climatological annual mean air temperature derived from all of the datasets (Fig. 5). LZU and CMA exhibit a consistent pattern with highlighting mountainous regions such as the Tianshan and Qilian Mountains. LZU, in the northern part of China, exhibits a higher temperature compared to CMA (CMA−LZU in the bottom of Fig. 5). This might be caused by extended stations in Mongolia involved in the interpolation; however, the differences are concentrated within the relatively narrow range of ± 1 °C. In addition, it is noticeable that the temperature patterns derived from site-based interpolation are much more similar than those from atmospheric model-based simulation

Fig. 5 Spatial distribution of climatological annual mean (1979–2008) air temperature-derived datasets (unit: °C). The graph on the lower right (CMA−LZU) is the difference between annual mean CMA and LZU

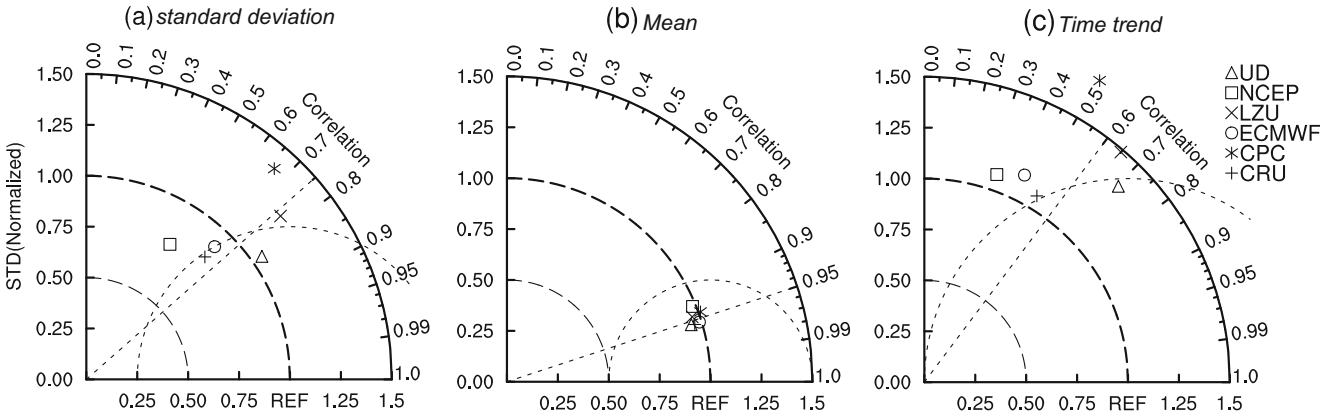

Fig. 4 Taylor diagram illustrating comparisons of monthly air temperature datasets. **a** The *standard deviation* index. **b** The *mean* index. **c** The *time trend* index (see Eq. (11) in Sect. 2.2). In each sub figure, the X-Y coordinates both represent the standard deviation derived from each index. The more close the symbol approaches to the referenced dataset CMA (REF has R = 1, STD_{ratio} = 1 and RMSE = 0, see Eq. (12) in Sect. 2.2) in graph, from the perspective of this index, the more similar the dataset represented by this symbol to the REF, and vice versa

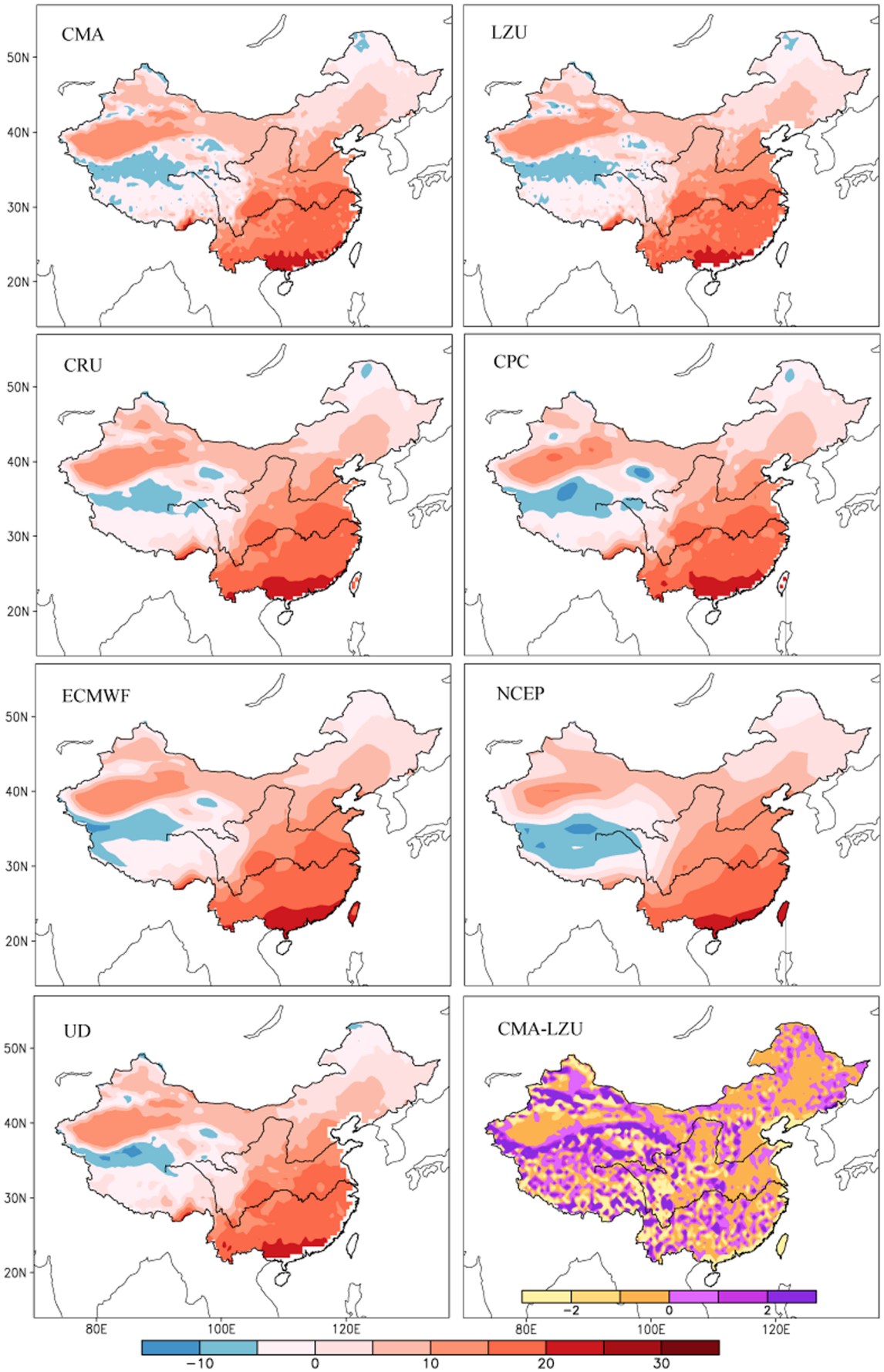
CMA
LZU
CRU
CPC
ECMWF
NCEP
UD
CMA-LZU
50N
40N
30N
20N
80E
100E
120E
−10
0
10
20
30
−2
0
2

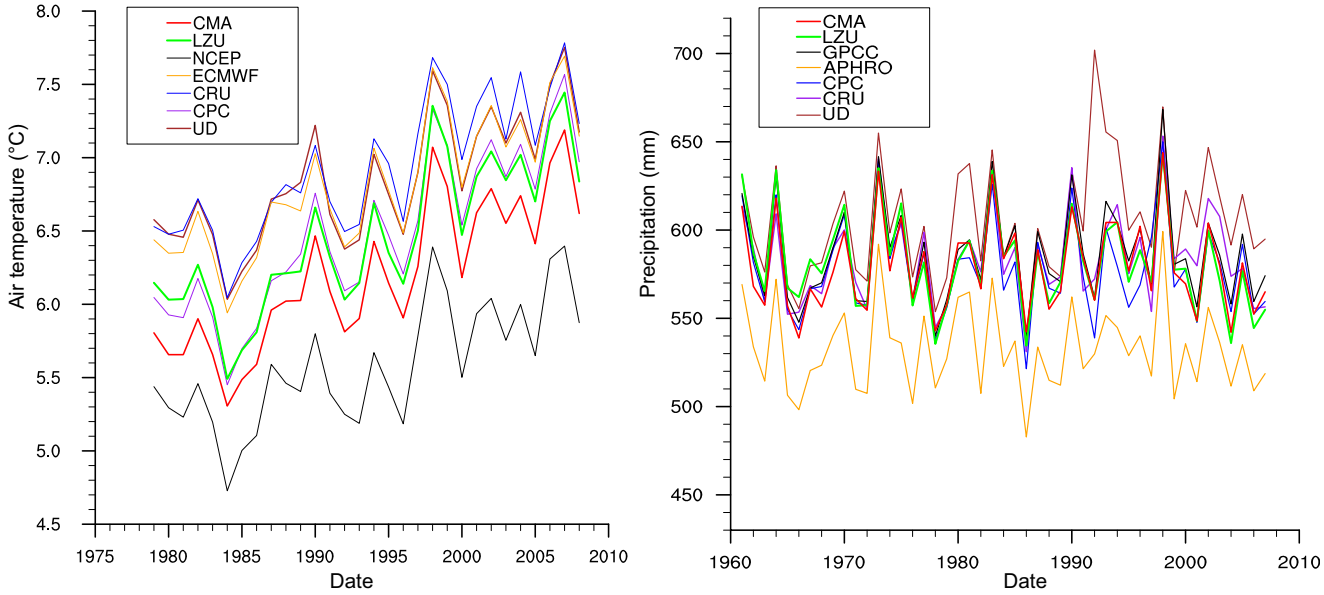

Fig. 6 Time series of annual mean air temperature (°C) (**a**) and precipitation (mm) (**b**) for all datasets in China

results. Compared with NCEP modeling data, the ECMWF are closer to the station data especially in the northwestern and Tibetan regions.

Comparisons of time series of monthly air temperature dataset are shown in Fig. 6a. The variations in the absolute value of annual air temperature are obvious for all of the datasets. The mean values for UD, CRU, and ECMWF are relatively high (6.9 °C, 7.0 °C, and 6.8 °C respectively), while those for LZU, CPC, and CMA are intermediate (6.5 °C, 6.5 °C, and 6.2 °C respectively), and that for NCEP is relatively low (5.6 °C). The linear regression coefficients (calculated by using the RegCoef command) for air temperature in time series from all datasets had positive values, indicating that all of the records provided an overall warming trend with the significant confidence of 95%. CPC provided the highest warming rate of 0.31 °C/10 year, followed by CMA with rate of 0.27 °C/10 year, LZU, CRU, and ECMWF with the same warming rate of 0.23 °C/10 year, and UD with rate of 0.20 °C/10 year and NECP with rate of 0.15 °C/10 year. However, the changing trends of annual mean temperature derived from various datasets are consistent with each other. The annual temperatures all increased and showed a small peak in 1982. Then, they all decreased and were at minimum in 1984. After that, they all increased rapidly with small fluctuations and peaked at high values in 1998. These peaks maintained with small fluctuations until 2006 and started to decline in 2007.

Comparisons of monthly precipitation were made during 1961–2007 period, since the total number of national meteorological stations in China stabilized in 1960 and the APHRO dataset was updated until 2007. Figure 7 illustrates a Taylor diagram of *standard deviation*, *mean*, and *time trend* indices (see Eq. (11)) derived from the various precipitation datasets.

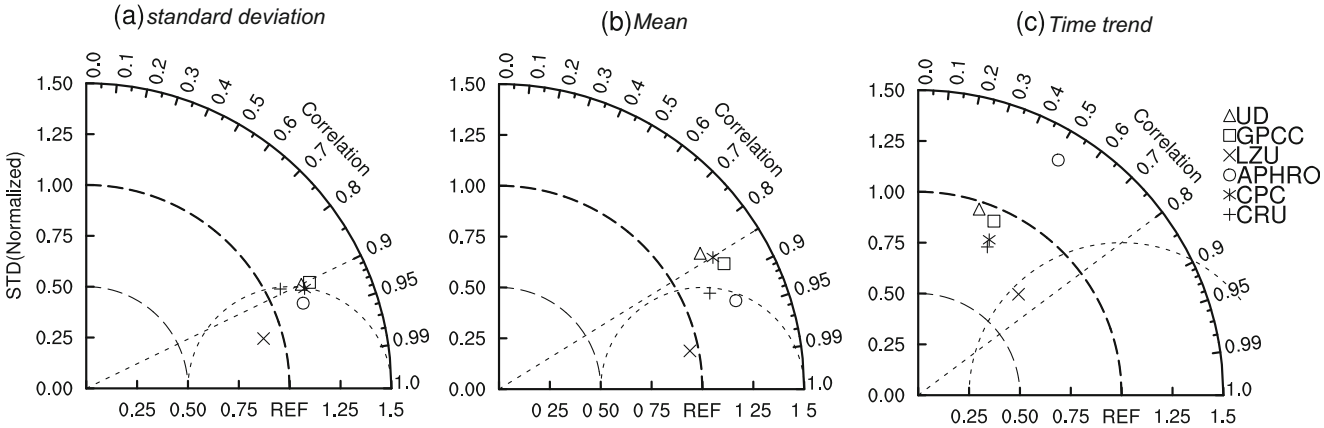

Fig. 7 Taylor diagram comparing the various precipitation datasets. **a** The *standard deviation* index. **b** The *mean* index. **c**The *time trend* index (see Eq. (11) in Sect. 2.2). In each sub figure, the X-Y coordinates both represent the standard deviation derived from each index. The more close the symbol approaches to referenced dataset CMA (REF with R = 1, STD_{ratio} = 1 and RMSE = 0, see Eq. (12) in Sect. 2.2) in graph, from the perspective of this index, the more similar the dataset represented by this symbol to the REF, and vice versa

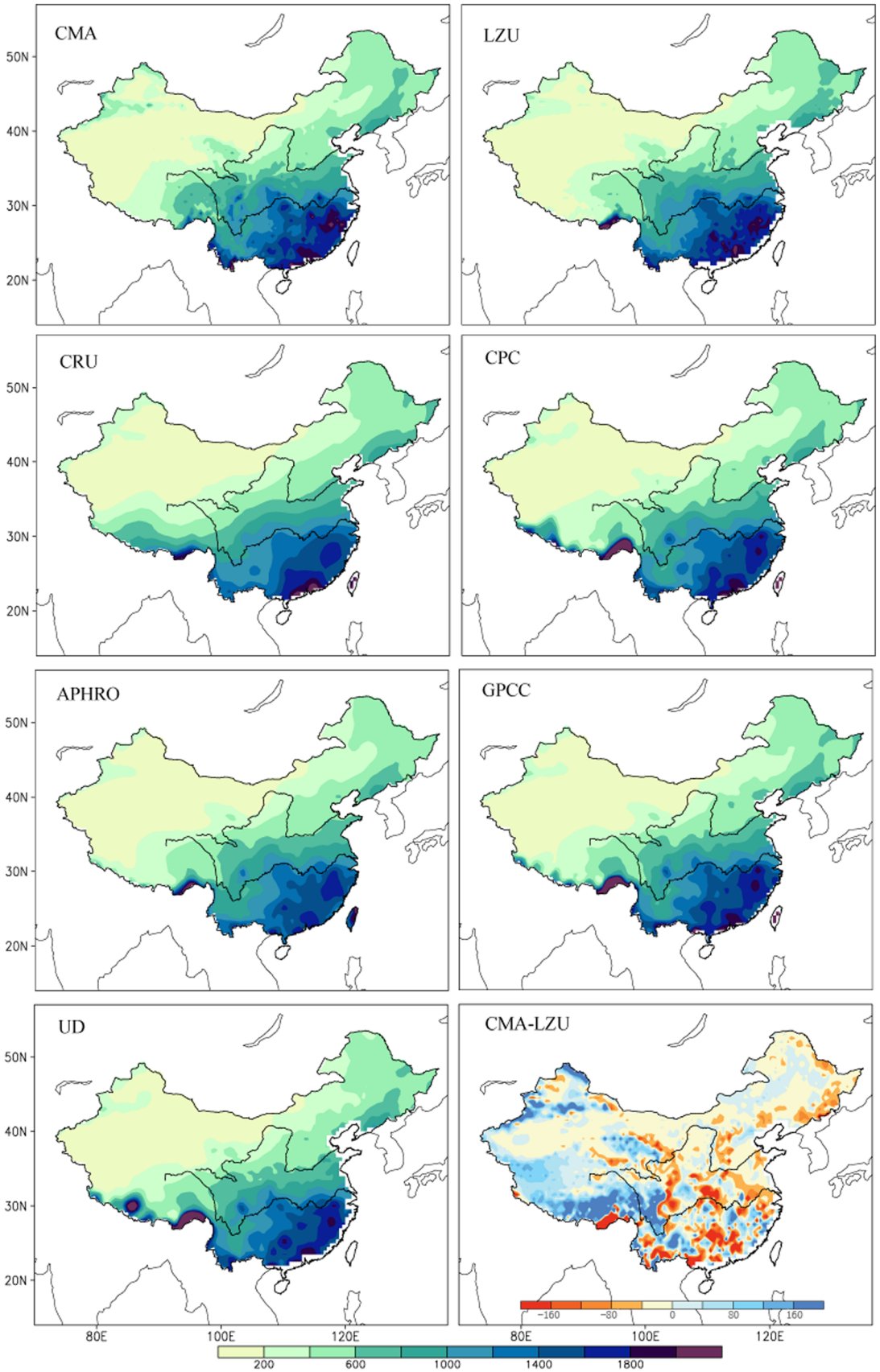

Fig. 8 Spatial distribution of mean annual (1961–2007) precipitation for datasets in China (unit: mm). The graph on the lower right (CMA−LZU) is the difference between these mean annual CMA and LZU

Table 4 Comparison of LZU0025 with the CAMP Tibet meteorology station dataset during the 2003–2004 period

Station	Latitude	Longitude	Air temperature		Precipitation	
			Bias (°C)	Correlation	Bias (mm)	Correlation
Gaize	32.30	84.05	0.6	0.998*	0.8	0.987*
MS3608	31.23	91.78	0.7	0.999*	−7.1	0.423
ANNI	31.25	92.17	−0.4	0.998*	−29.6	0.828*
D66	35.52	93.78	−1.0	0.998*	−1.6	0.873*
BJ-Tower	31.37	91.90	−0.5	0.998*	−28.4	0.892*
D105	33.06	91.94	−0.6	0.999*	−13.7	0.896*
MS3478	31.93	91.71	−0.7	0.999*	−16.6	0.895*
Amedo	32.24	91.62	−0.6	0.994*	−17.1	0.733

Without asterisk, the correlation relationship was non-significant

*Passing the statistical significant test at a level of 0.01

For the *standard deviation* index (Fig. 7a), the correlations between all of the datasets and CMA are high ($R > 0.9$), and LZU with CMA has the highest R of 0.97. The STDs for LZU, APHRO, and CRU are significantly closer to STD of CMA than those of UD, GPCC, and CPC, and the RMSEs of all of the datasets are close to that of CMA especially for LZU (RMSE < 0.5). With regard to the *standard deviation* index, LZU, CPC, GPCC, and UD are more similar to CMA than are CRU and APHRO. For the *mean* index (Fig. 7b), the correlations of LZU and APHRO with CMA are the highest ($R > 0.94$), while the STD for LZU is closer to that of CMA than that of APHRO, and the RMSE of LZU with CMA is the lowest (RMSE = 0.2). With regard to the *time trend* index (Fig. 7c), the correlation of LZU with CMA is the highest ($R = 0.75$), and the correlations of the other datasets with CMA are centralized with only minor differences ($R = 0.3$–0.5). The STD for LZU is closest to that of UD and GPCC, followed by CPC and CRU, and LZU and APHROS take the last place. LZU has the smallest RMSE (= 0.74) with CMA, and other datasets have similar great RMSE (> 0.75). In summary, LZU, APHRO, CPC, CRU, and GPCC are closer to CMA, and UD biased obviously.

Spatial distributions of climatological annual mean precipitation derived from all of the datasets are illustrated in Fig. 8. All datasets show the similar decreasing of annual precipitation from southeastern to northwestern (< 200 mm). With more stations in the mountainous area interpolated for CMA and LZU, CMA and LZU provide high annual mean precipitation amount (> 200 mm) in Tianshan and Qilian Mountains in northwest part of China. Compared with CMA, the precipitation derived from LZU in the foothills of the Himalayan Mountain exceeds 2000 mm, as is also the case for CRU, CPC, APHRO, and GPCC, due to the interpolation containing station data in neighboring countries. Thus, it is clear that the optimized LZU dataset accurately describes the climatic conditions close to the national border. Time series of monthly precipitation datasets displayed in Fig. 6b shows that UD provides the greatest annual mean precipitation amount (604 mm); CMA, LZU, GPCC, CPC, and CRU gives similar mean precipitation amount (579 mm, 578 mm, 586 mm, 578 mm, and 583 mm, respectively), and APHRO provides the lowest annual mean precipitation amount (532 mm) (Fig. 6b). All of the precipitation datasets exhibit a similar pattern of fluctuations superimposed on a long-term trend (Fig. 6b). It can be seen that LZU is the most similar to CMA, and LZU can well depict the temporal variations of air temperature and precipitation in China.

Further, the LZU0025 with a high spatial resolution was compared with the CAMP Tibet surface meteorology station dataset. Table 4 shows during the 2003–2004 period, the correlation between these two datasets for each station was high especially for air temperature element. While it is noted that the correlation for precipitation was not significant for few stations and the comparison was only confined in this short time period. A caution should be taken when using LZU0025 precipitation dataset in this region, and it is suggested that the accuracy of LZU00025 precipitation dataset needs to be further checked once local station data on similar mountainous and remote areas are accessible.

The above results suggested that LZU performs well and LZU0025 can be so far reliable. LZU0025 with a much higher spatial resolution provides more information about local climate state. To illustrate the advantage of LZU0025, here, we give an example of comparisons about the spatial distribution of climate types in China deduced from different datasets. The Köppen and Trewartha climate classification (K-T) (Trewartha and Horn 1980) was used, which was the modification of Köppen's original approach on adjusting both the original temperature criteria and the thresholds separating wet and dry climates (Belda et al. 2014). Figure 9 shows that LZU0025 and other datasets share a similar distribution pattern of climate type during 1991–2000 period, and the main types covering China are the arid and semiarid climate (BW and BS), subtropical humid and subtropical winter dry climate (Cf and Cw),

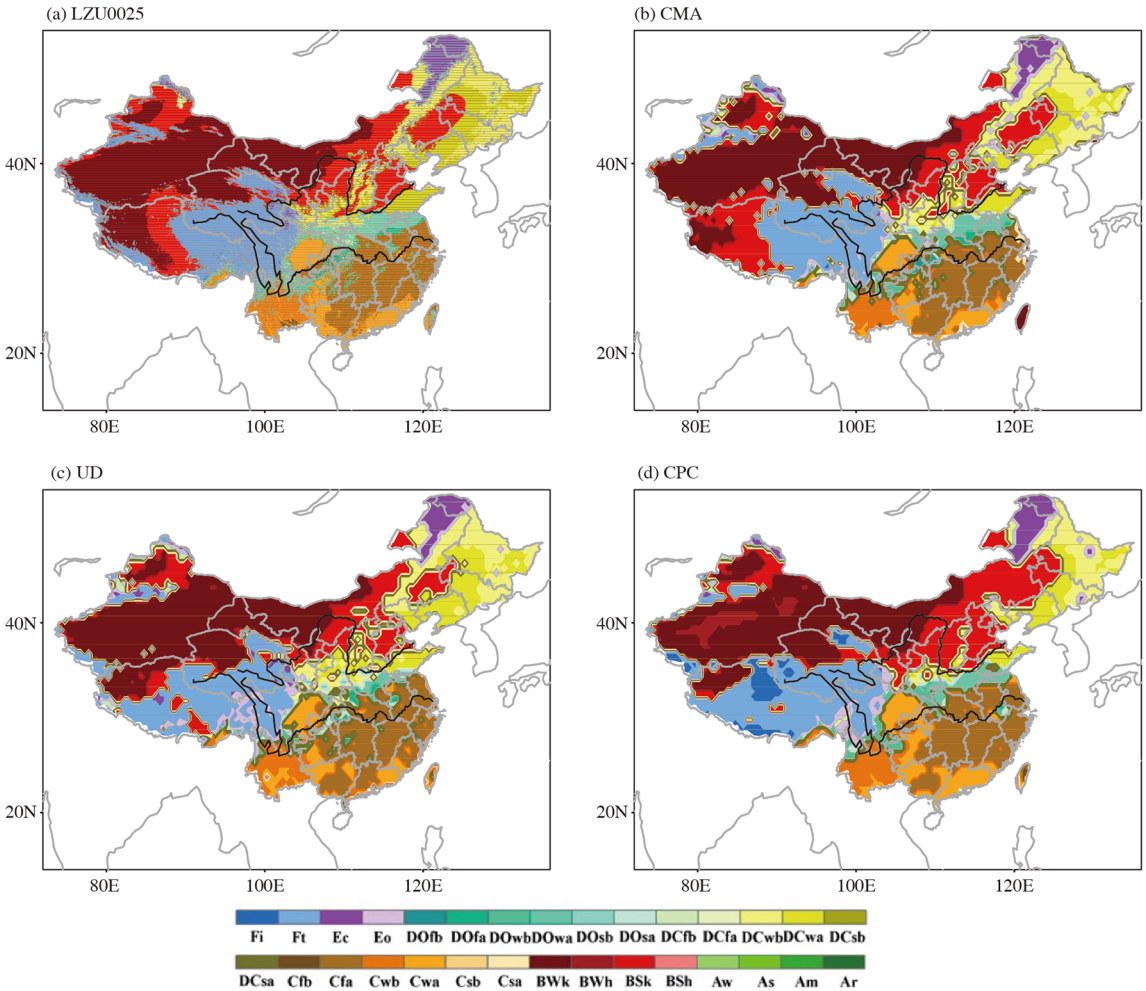

Fig. 9 Spatial distribution of the K-T climate types in China (1991–2000). K-T means Köppen and Trewartha climatic classification (Trewartha and Horn, 1980)

temperature continental and oceanic climate (Dc and Do), and tundra climate (Ft). This consistent distribution further illustrates the reliability of LZU0025. Figure 9 also shows that LZU0025 and CMA provided more detailed climate type than that from global datasets. UD and CPC only deduced the tundra climate (Ft) in the southwest of China, while for LZU0025 and CMA, besides that, they depicted the dry climate of arid and semi-arid types (BWk and BSk) (Fig. 9). Compared with CMA, LZU0025 could provide more information of the distribution of local climate. LZU0025 identified the tundra climate (Ft) along the west of Himalayan Mountain as the global datasets showed, while CMA could not (Fig. 9), and this was attributed to the LZU0025 interpolation considering the stations in the neighboring countries. What is more, it is seen that LZU0025 with higher spatial resolution provided more detailed information of climate type, which is represented by the occurrence of scattered points from LZU0025 in Fig. 9. Taking climate types in the region of 35°N–40°N and 95°E–105°E as an example, it was found that LZU0025 could deduce the subpolar continental climate (coldest month < −10 °C) due to its higher resolution while CMA and other datasets could not (Fig. 9). Therefore, the high spatial resolution of LZU0025 is obviously a major advantage.

4 Conclusions

This paper used extended meteorological station dataset and ANUSPLIN software to construct monthly air temperature and precipitation datasets with a spatial resolution of 0.025° in China (named LZU0025) and corresponding error datasets, for the interval Jan 1951 to Dec 2011. The accuracy of LZU0025 was evaluated by analyzing diagnostic statistics for climatic surface fitting and errors statistics based on comparisons between interpolated values against withheld stations data. Furthermore, taking the dataset from China Meteorological Administration (CMA) as the reference, LZU0025 was compared with other existing datasets. The explicit procedure was comparing three indices of *standard deviation*, *mean*, and *time trend* derived from these datasets in Taylor diagrams. The

results indicated that the constructed LZU0025 is reliable (accessible from https://doi.pangaea.de/10.1594/PANGAEA.895742) and can be used as a basis for research on regional climatic change monitoring, regional hydrological cycle simulation, and precision agriculture modulation under global climate change. The next step is to use LZU0025 to analyze the climate types changing in China, which will add extra evidences on understanding climate change.

Acknowledgements We thank the editor and two anonymous reviewers for their constructive comments, which have led to improvement of this manuscript. We also thank our previous colleague Zhiping Long for providing the NCL code about dataset comparison.

Funding information This work was jointly supported by the National Natural Science Foundation of China (NSFC) (Grant No. 41790421, 41877446), and Fundamental Research Funds for the Central Universities (Grant No. lzujbky-2018-140).

References

Anwar MR, Li Liu D, Macadam I, Kelly G (2013) Adapting agriculture to climate change: a review. Theor Appl Climatol 113:225–245. https://doi.org/10.1007/s00704-012-0780-1

Belda M, Holtanová E, Halenka T, Kalvová J (2014) Climate classification revisited: from Köppen to Trewartha. Clim Res 59:1–13. https://doi.org/10.3354/cr01204

Brown JR, Power SB, Delage FP, Colman RA, Moise AF, Murphy BF (2011) Evaluation of the South Pacific convergence zone in IPCC AR4 climate model simulations of the twentieth century. J Clim 24:1565–1582. https://doi.org/10.1175/2010JCLI3942.1

Chen S, Chen X, Xu J (2016) Impacts of climate change on agriculture: evidence from China. J Environ Econ Manage 76:105–124. https://doi.org/10.1016/j.jeem.2015.01.005

Ciabatta L, Brocca L, Moramarco T, Wagner W (2015) Comparison of different satellite rainfall products over the Italian territory. In: Lollino G, Arattano M, Rinaldi M, Giustolisi O, Marechal JC, Grant G (eds) Engineering Geology for Society and Territory-Volume 3, Torino. Springer, Cham, pp 623–626. https://doi.org/10.1007/978-3-319-09054-2_124

Conti FL, Hsu KL, Noto LV, Sorooshian S (2014) Evaluation and comparison of satellite precipitation estimates with reference to a local area in the Mediterranean Sea. Atmos Res 138:189–204. https://doi.org/10.1016/j.atmosres.2013.11.011

Craven P, Wahba G (1978) Smoothing noisy data with spline functions. Numer Math 31:377–403. https://doi.org/10.1007/BF01404567

Dee D, Uppala S, Simmons A, Berrisford P, Poli P, Kobayashi S, Andrae U, Balmaseda M, Balsamo G, Bauer P (2011) The ERA-interim reanalysis: configuration and performance of the data assimilation system. Q J Royal Meteorol Soc 137:553–597. https://doi.org/10.1002/qj.828

Ding Y, Ren G, Zhao Z, Xu Y, Luo Y, Li Q, Zhang J (2007) Detection, causes and projection of climate change over China: an overview of recent progress. Adv Atmos Sci 24:954–971. https://doi.org/10.1007/s00376-007-0954-4

Fan Y, Van den Dool H (2008) A global monthly land surface air temperature analysis for 1948–present. J Geophys Res Atmos 113:1–18. https://doi.org/10.1029/2007JD008470

Feng S, Hu Q, Qian W (2004) Quality control of daily meteorological data in China, 1951–2000: a new dataset. Int J Climatol 24:853–870. https://doi.org/10.1002/joc.1047

Harris I, Jones P, Osborn T, Lister D (2014) Updated high-resolution grids of monthly climatic observations—the CRU TS3. 10 dataset. Int J Climatol 34:623–642. https://doi.org/10.1002/joc.3711

Hessels TM (2015) Comparison and validation of several open access remotely sensed rainfall products for the Nile Basin. Master, TU Delft, Delft University of Technology

Houghton J (2002) The physics of atmospheres, Third edn. Cambridge University Press, Cambridge. https://doi.org/10.1002/qj.200212858322

Huang W, Chen J, Zhang X, Feng S, Chen F (2015) Definition of the core zone of the "westerlies-dominated climatic regime", and its controlling factors during the instrumental period. Sci China Earth Sci 58:676–684. https://doi.org/10.1007/s11430-015-5057-y

Hutchinson MF (1991) The application of thin plate smoothing splines to continent-wide data assimilation. In: Jasper JD (ed) Data assimilation systems. BMRC Res. Rep. No. 27. Bureau of Meteorology, Melbourne, pp 104–113

Hutchinson, MF (1993) On thin plate splines and kriging. In: Tarter ME, Lock MD (ed) Computing Science and Statistics, vol. 25. University of California, Berkeley. pp. 55–62. https://www.researchgate.net/publication/302558932_On_thin_plate_splines_and_kriging. Accessed 5 Sep 2018

Hutchinson MF (1995) Interpolating mean rainfall using thin plate smoothing splines. Int J Geogr Inf Sci 9:385–403. https://doi.org/10.1080/02693799508902045

Hutchinson MF (1998a) Interpolation of rainfall data with thin plate smoothing splines. Part I: Two dimensional smoothing of data with short range correlation. GIDA 2:139–151

Hutchinson MF (1998b) Interpolation of rainfall data with thin plate smoothing splines. Part II: Analysis of topographic dependence. GIDA 2:152–167

Hutchinson MF, Gessler P (1994) Splines—more than just a smooth interpolator. Geoderma 62:45–67. https://doi.org/10.1016/0016-7061(94)90027-2

Hutchinson MF, McKenney DW, Lawrence K, Pedlar JH, Hopkinson RF, Milewska E, Papadopol P (2009) Development and testing of Canada-wide interpolated spatial models of daily minimum-maximum temperature and precipitation for 1961-2003. J Appl Meteorol Clim 48:725–741. https://doi.org/10.1175/2008JAMC1979.1

Hutchinson MF, Xu T (2004) ANUSPLIN version 4.2 user guide vol 54. Centre for Resource and Environmental Studies, The Australian National University, Canberra

Hutchinson MF, Xu T (2013) ANUSPLIN version 4.4 user guide. The Australian National University, Fenner School of Environment and Society, Canberra

IPCC (2013) The physical science basis. Contribution of working group I to the fifth assessment report of the intergovernmental panel on climate change. Cambridge University Press, Cambridge

Ishikawa H (2011) CAMP: Tibet surface meteorology and radiation data set. Version 1.0. UCAR/NCAR - Earth Observing Laboratory. https://data.eol.ucar.edu/dataset/76.127. Accessed 2 Sep 2018

Kalnay E, Kanamitsu M, Kistler R, Collins W, Deaven D, Gandin L, Iredell M, Saha S, White G, Woollen J (1996) The NCEP/NCAR 40-year reanalysis project. Bull Amer Meteor Soc 77:437–471. https://doi.org/10.1175/1520-0477(1996)077

Kim J, Waliser DE, Mattmann CA, Mearns LO, Goodale CE, Hart AF, Crichton DJ, McGinnis S, Lee H, Loikith PC (2013) Evaluation of the surface climatology over the conterminous United States in the North American regional climate change assessment program hindcast experiment using a regional climate model evaluation system. J Clim 26:5698–5715. https://doi.org/10.1175/JCLI-D-12-00452.1

Li Q, Zhang H, Liu X, Huang J (2004) Urban heat island effect on annual mean temperature during the last 50 years in China. Theor Appl Climatol 79:165–174. https://doi.org/10.1007/s00704-004-0065-4

Li Z, Liu Z, Anderson W, Yang P, Wu W, Tang H, You L (2015) Chinese rice production area adaptations to climate changes, 1949–2010. Environ Sci Technol 49:2032–2037.https://doi.org/10.1021/es505624x

Liu C, Huang W, Feng S, Chen JH, Zhou AF (2018) Spatiotemporal variations of aridity in China during 1961-2015: decomposition and attribution. Sci Bull 63:1187–1199. https://doi.org/10.1016/j.scib.2018.07.007

Liu Z, Yang P, Tang H, Wu W, Zhang L, Yu Q, Li Z (2015) Shifts in the extent and location of rice cropping areas match the climate change pattern in China during 1980–2010. Reg Environ Chang 15:919–929. https://doi.org/10.1007/s10113-014-0677-x

Liu Z, Zhang G, Yang P (2016) Geographical variation of climate change impact on rice yield in the rice-cropping areas of Northeast China during 1980–2008. Sustainability 8:670. https://doi.org/10.3390/su8070670

Ma H, Xie S, Klein S, Williams K, Boyle J, Bony S, Douville H, Fermepin S, Medeiros B, Tyteca S (2014) On the correspondence between mean forecast errors and climate errors in CMIP5 models. J Clim 27:1781–1798. https://doi.org/10.1175/JCLI-D-13-00474.1

Matsuura K, Willmott CJ (2009) Terrestrial precipitation: 1900–2010 gridded monthly time series. Newark: Center for Climatic Research, Department of Geography, University of Delaware http://climate.geog.udel.edu/~climate/. Accessed 5 Jan 2015

Menne MJ, Williams CN (2009) Homogenization of temperature series via pairwise comparisons. J Clim 22:1700–1717. https://doi.org/10.1175/2008JCLI2263.1

Pai D, Sridhar L, Rajeevan M, Sreejith O, Satbhai N, Mukhopadhyay B (2014) Development of a new high spatial resolution (0.25× 0.25) long period (1901–2010) daily gridded rainfall data set over India and its comparison with existing data sets over the region. Mausam 65:1–18

Piao S, Ciais P, Huang Y, Shen Z, Peng S, Li J, Zhou L, Liu H, Ma Y, Ding Y (2010) The impacts of climate change on water resources and agriculture in China. Nature 467:43–51. https://doi.org/10.1038/nature09364

Schneider U, Becker A, Finger P, Meyer-Christoffer A, Rudolf B, Ziese M (2011) GPCC full data reanalysis version 6.0 at 0.5: monthly land-surface precipitation from rain-gauges built on GTS-based and historic data. doi: https://doi.org/10.5676/DWD_GPCC/FD_M_V6_050

Schneider U, Becker A, Finger P, Meyer-Christoffer A, Ziese M, Rudolf B (2014) GPCC's new land surface precipitation climatology based on quality-controlled in situ data and its role in quantifying the global water cycle. Theor Appl Climatol 115:15–40. https://doi.org/10.1007/s00704-013-0860-x

Shen M, Piao S, Cong N, Zhang G, Jassens IA (2015) Precipitation impacts on vegetation spring phenology on the Tibetan plateau. Glob Change Biol 21:3647–3656. https://doi.org/10.1111/gcb.12961

Song Y, Wang C, Ren G, Zhao Y, Linderholm HW (2015) The relative contribution of climate and cultivar renewal to shaping rice yields in China since 1981. Theor Appl Climatol 120:1–9. https://doi.org/10.1007/s00704-014-1089-z

Taylor KE (2001) Summarizing multiple aspects of model performance in a single diagram. J Geophys Res Atmos 106:7183–7192. https://doi.org/10.1029/2000JD900719

Taylor KE (2005) Taylor diagram primer. Program For Climate Model Diagnosis and Intercomparison (PCMDI), https://pcmdi.llnl.gov/staff/taylor/CV/Taylor_diagram_primer.pdf?id=87. Accessed 5 Jan 2015

Trewartha G, Horn L (1980) Köppen's classification of climate. In: Introduction to climate. 5th edn. McGraw-Hill, New York, pp 397–403

Wahba G (1983) Cross validated spline methods for the estimation of multivariate functions from data on functionals.In: H.A. David and H.T. David, (eds.) Statistics, an Appraisal, Proceedings of the Iowa State University Statistical Laboratory 50th Anniversary Conference. The Iowa State University Press. doi:https://doi.org/10.1016/B978-0-444-42697-0.50023-0

Wahba G (1986) Partial and interaction splines for the semiparametric estimation of functions of several variables. In: Boardman TJ (ed) Computer science and statistics: proceedings of the 18th symposium on the Interface. American Statistical Association, Washington, DC, pp 75–80

Wahba G (1990) Spline models for observational data. In: CBMS-NSF Regional Conference Series in Applied Mathematics. Philadelphia, PA 19104–2688.1990SIAM. doi:https://doi.org/10.1137/1.9781611970128

Wahba G, Wendelberger J (1980) Some new mathematical methods for variational objective analysis using splines and cross validation. Mon Weather Rev 108:1122–1143. https://doi.org/10.1175/1520-0493(1980)108<1122:SNMMFV>2.0.CO;2

Wen X, Wang S, Zhu J, Viner D (2006) An overview of China climate change over the 20th century using UK UEA/CRU high resolution grid data. Chin J Atmos Sci 30:894 (In Chinese)

Wu X, Huang W, Chen F (2014) Construction and application of monthly air temperature and precipitation gridded datasets high resolution (0.025× 0.025) over China during 1951–2012. J Lanzhou Univ (Nat Sci) 50:1–8 (In Chinese)

Xiao D, Qi Y, Shen Y, Tao F, Moiwo JP, Liu J, Wang R, Zhang H, Liu F (2016) Impact of warming climate and cultivar change on maize phenology in the last three decades in North China plain. Theor Appl Climatol 124:653–661. https://doi.org/10.1007/s00704-015-1450-x

Xu Y, Gao X, Sheng Y, Xu C, Shi Y (2009) A daily temperature dataset over China and its application in validating a RCM simulation. Adv Atmos Sci 26:763–772. https://doi.org/10.1007/s00376-009-9029-z

Yatagai A, Kamiguchi K, Arakawa O, Hamada A, Yasutomi N, Kitoh A (2012) APHRODITE: constructing a long-term daily gridded precipitation dataset for Asia based on a dense network of rain gauges. Bull Am Meteorol Soc 93:1401–1415. https://doi.org/10.1175/BAMS-D-11-00122.1

Yu J, Shen Y, Pan Y (2015) Comparative assessment between the daily merged precipitation dataset over China and the world's popular counterparts. Acta Meteorol Sin 73:394–410. https://doi.org/10.11676/qxxb2015.033 (In Chinese)

Zhang Q, Ruan X, Xiong A (2009) Establishment and assessment of the grid air temperature data sets in China for the past 57 years. J Appl Meteorol Sci 20:385–393. https://doi.org/10.3969/j.issn.1001-7313.2009.04.001 (In Chinese)

Zhang X, Shao Ja, Luo H (2011) Spatial interpolation of air temperature with ANUSPLIN in three gorges reservoir area. In: International conference on remote sensing, Environment and Transportation Engineering (RSETE). IEEE, pp 3465–3468. doi:https://doi.org/10.1109/RSETE.2011.5965057

Zhang Z, Song X, Tao F, Zhang S, Shi W (2016) Climate trends and crop production in China at county scale, 1980 to 2008. Theor Appl Climatol 123:291–302. https://doi.org/10.1007/s00704-014-1343-4

Zhao J, Yang X, Lv S, Liu Z, Wang J (2014) Variability of available climate resources and disaster risks for different maturity types of spring maize in Northeast China. Reg Environ Chang 14:17–26. https://doi.org/10.1007/s10113-013-0476-9

Zhou W, Shi J, Mu H (2010) Climate change characteristics of winter temperature and precipitation in eastern China. Resour Sci 6:015. https://doi.org/10.1155/2017/4635280 (In Chinese)